Journal of NAMP 73 (2026) 1-12

The Nigerian Association of Mathematical Physics

Journal homepage: https://nampjournals.org.ng

Geophysical and Statistical Analysis of Solar Wind and Geomagnetic Conditions During FAST-ESR Ion-Upwelling Conjunctions

T. W. David[1,2,*], E. O. Adetunji[3], C. M. Michael[4,2], D. M. Wright[2], A. E. Ajetunmobi[1], A. T. Talabi[1]

[1]*Department of Physics, Olabisi Onabanjo University, Ago-Iwoye, Nigeria*
[2]*School of Physics and Astronomy, University of Leicester, Leicester, UK*
[3]*Department Basic Science, Babcock University, Ilishan, Nigeria*
[4]*Faculty of Art, Science and Technology, University of Northampton, Northampton, UK*
*Corresponding author: david.timothy@oouagoiwoye.edu.ng

ARTICLE INFO

Article history:
Received xxxxx
Revised xxxxx
Accepted xxxxx
Available online xxxxx

Keywords:
ionosphere,
ion upflow,
geophysical conditions
magnetosphere

ABSTRACT

This study examines how solar wind and geomagnetic conditions drive heavy-ion outflow from the topside ionosphere, which influences atmospheric loss and magnetospheric dynamics. Using FAST satellite and EISCAT Svalbard Radar data during seven magnetic conjunction events with previously identified ion upwelling, the authors analyzed OMNI solar wind data and geomagnetic indices. Two representative events are highlighted: a nightside conjunction on 2002-01-20 during a substorm expansion phase with strongly southward IMF and AL exceeding -350 nT, and a dayside conjunction on 2006-03-18 during a corotating interaction region featuring variable solar wind and a two-step southward Bz turning. Across all events, 2006-03-18 showed the greatest solar wind variability and strongest dayside reconnection coupling, while 2005-09-12 exhibited the most solar wind–magnetosphere energy transfer in the sample. The findings are consistent with the established view that southward IMF and enhanced dynamic pressure promote ion energisation via reconnection-driven Joule heating and electron precipitation.

1. Introduction

The Earth's near-space environment can be viewed as a coupled plasma system that is driven and sustained by the interaction of solar and geomagnetic fields [1, 2]. The solar wind, a supersonic plasma sheet that originates from the Sun, spreads throughout the heliosphere with the interplanetary magnetic field (IMF). Upon interaction with Earth's intrinsic magnetic field, the wind shapes the magnetosphere to a compressed size of about 10 Earth radii (R_E) on the dayside and a tail extending several hundreds of R_E on the nightside [3].

*Corresponding author: T. W. David
E-mail address: david.timothy@oouagoiwoye.edu.ng
https://doi.org/10.60787/jnamp.vol73no.724

The overall configuration and state of the magnetosphere are controlled by momentum, mass, and energy coupling with the solar wind, which is predominantly achieved through magnetic reconnection [4, 5], a process that is most efficient when the IMF and geomagnetic fields are oppositely directed. Viscous coupling [6] also exists but typically plays a secondary role.

Two sources supply the plasma for the magnetosphere: direct entry of solar wind plasma through reconnection and upward transport of ionospheric plasma from the upper atmosphere [7, 8]. The process of ion escape from the ionosphere into the magnetosphere plays a key role in setting the global plasma density, composition, and magnetospheric response to solar wind forcing [9, 10]. It is comprised of an initial stage, ion upwelling, which is characterised by the upward motion of ions that have not yet reached escape speed. Once sufficiently energised, these ions become outflowing plasma that enters the magnetosphere and contributes to the global mass loading and circulation of magnetospheric plasma [11–13].

Ion energization and escape are a result of a combination of soft electron precipitation, ambipolar electric fields, Joule heating, and wave–particle interactions [14, 15]. These processes allow heavy ions to overcome gravitational and collisional confinement to produce measurable fluxes along open magnetic field lines. ESR (European Incoherent Scatter Svalbard Radar) and satellite observations have shown that ion upflow is present at all local times, with a maximum near local noon under enhanced solar illumination and reconnection conditions [16, 17]. Recent advances in modelling and simulation have enabled improved quantitative understanding of ionospheric outflow processes through inclusion of kinetic effects, wave–particle coupling, and geomagnetic activity drivers [18, 19].

Empirical studies have shown that ion upflow intensity varies with solar and geomagnetic conditions, including IMF orientation and solar wind dynamic pressure, and substorm activity [7, 20]. Using a statistical classification of ESR ion-flux profiles obtained during the 2007 International Polar Year campaign, David et al. [17] identified low-, medium-, and high-flux upflow events occurring when the upflow flux was around 10^13 m^(-2) s^(-1), which defines the upflow–outflow regime transition. During the International Polar Year (IPY) 2007 campaign, David et al. [22] showed that upflow-associated plasma noise is reduced near local noon and during summer months, and enhanced around 17:00–18:00 LT, indicating strong diurnal and seasonal dependencies. David [23] while investigating quiet and geomagnetic storms periods showed that either period could trigger elevated ionospheric storms. The ionosphere's response to geomagnetic storms is different between stations, implying localized variations in solar wind–magnetosphere–ionosphere coupling efficiency [24, 25]. The IMF By component was shown to vary cusp displacement, causing dawn–dusk asymmetries that affect upflow occurrence [20, 26].

Although considerable progress has been made on observational and modelling studies, uncertainties remain regarding how specific geophysical conditions – magnetic reconnection efficiency, substorm activity and the rate of solar wind–magnetosphere energy coupling – modulate the transition from ion upwelling to magnetospheric outflow. Resolving these uncertainties requires coordinated multi-instrument analyses of the upstream driver and the ionospheric response. In this work, we focus specifically on the upstream forcing during the seven FAST-ESR magnetic conjunctions catalogued by David et al. [31], in which simultaneous ion upwelling above the ESR was confirmed using the ion-flux threshold convention of David et al. [17]. Rather than re-establishing the upwelling identifications, we take those events as given and characterise the solar wind, IMF and geomagnetic conditions that prevailed during each conjunction. Two events are then examined in detail as case studies (a nightside conjunction on 2002-01-20 and a dayside conjunction on 2006-03-18), after which we present the central tendency, dispersion and Milan et al. [30] dayside reconnection coupling function across all seven conjunctions. Our aim is to identify which interplanetary and geomagnetic regimes accompany observed upwelling and to provide a baseline characterisation of the driving conditions for use in future modelling and statistical studies.

2. Data and Methodology

High-resolution OMNI data set of solar wind plasma parameters at the bow shock region of the Earth, and also of energetic proton fluxes and geomagnetic activity indices, available at

http://omniweb.gsfc.nasa.gov/ow_min.html, were employed in this work. One minute resolution upstream solar wind plasma parameters from OMNIWeb comprising the solar wind speed, v_{sw}, the solar wind number density, n_{sw}, the dynamic pressure, P_{dyn}, the IMF components, B_x, B_y and B_z, as well as the downstream geomagnetic ring current index (Sym-H) and lower and upper auroral electrojet indices (AL and AU) were downloaded from the National Aeronautics and Space Administration (NASA) website.
The FAST satellite was a NASA Small Explorer mission operating from 1996 to 2009 in an elliptical polar orbit (350–4180 km altitude, 83° inclination), designed to observe the auroral acceleration region with high time resolution plasma and field instruments [11, 15]. In this work we use the FAST-ESR conjunction events catalogued by David et al. [31], in which simultaneous ion upwelling signatures were identified above the EISCAT Svalbard Radar at the magnetic footprint of the satellite.
The EISCAT Svalbard Radar (ESR) is a UHF (500 MHz) incoherent scatter radar located at Longyearbyen, Svalbard (78.15°N, 16.03°E geographic; ~75° magnetic latitude). It provides height-resolved profiles of electron density, electron and ion temperatures, and field-aligned ion velocity in the topside ionosphere [16, 17]. Throughout this work, an ion-upwelling event is defined, following Wahlund and Opgenoorth [21] and David et al. [17], as one in which the ESR field-aligned ion flux exceeds 10^{13} m^{-2} s^{-1}. The seven FAST–ESR conjunctions analysed here (Table 1) are those identified by David et al. [31] in which both instruments were operating simultaneously and this threshold was met above ~400 km altitude in the ESR field-aligned beam. Representative ESR ion-upflow profiles for the two case-study events (2002 01 20 and 2006 03 18) are reproduced in Figure 1 from David et al. [31], where the full ESR record for both events is presented.
Conjunction events are taken from David et al. [31]. As reported there, ~3000 FAST-ESR pass-overs occurred during the FAST mission lifetime (1996-2009), of which 283 occurred while the ESR was operating; among these, seven events met the upwelling flux threshold defined above and are the events catalogued in Table 1. The present work uses this set of seven conjunctions without modification.
To characterise the energy transferred from the solar wind into the magnetosphere we use the dayside reconnection coupling function of Milan et al. [30], which expresses the reconnection electric field as a function of the upstream solar wind speed, the transverse IMF magnitude and the IMF clock angle (Eq. 1, presented in Section 3.2). This formulation was selected over the ε-parameter and the Newell coupling function because it shows the highest reported correlation ($\rho \approx 0.9$) with the open polar cap flux and is therefore a direct proxy for the dayside reconnection rate [30].
For each conjunction we extract a six-hour OMNI window centred on the conjunction time (i.e. ±3 h around T_{conj}), which spans the typical lifetime of substorm growth, expansion and recovery and is sufficient to capture the IMF and pressure variations relevant to ion upwelling driving [3]. Within this window we compute, for each parameter, the mean (m), median (Q2), lower and upper quartiles (Q1, Q3) and standard deviation (SD) as measures of central tendency and dispersion. Because Q1 and Q3 are computed over the full six-hour window, which is symmetric about T_{conj}, they approximately summarise the conditions before and after the conjunction. Given the small number of events (N = 7), these statistics are reported as descriptive measures of each individual event rather than as the basis for inferential tests; an enlarged event sample, beyond the scope of this conjunction-defined dataset, would be required for inferential statistics.

3. Results and Discussion

The solar wind plasma parameters from OMNIWeb are investigated to analyse the coupling function, examine the dayside magnetic reconnection, and the nightside magnetospheric substorm levels, for the seven FAST-ESR events. The detailed observation of geophysical conditions of two distinct events, a nightside event (2002-01-20) and one of the dayside events (2006-03-18) is also presented. The date and universal time of the seven FAST-ESR conjunctions are shown in Table 1.

Table 1: Date and universal time of the seven FAST-ESR conjunction events

Date	1998-02-01	2002-01-20	2005-09-12	2005-09-18	2006-03-11	2006-03-18	2008-02-14
UT	11:30:34	22:20:55	11:25:01	10:48:00	09:21:54	08:09:23	12:07:05

The *SYM-H* ring current index, the *AL* and *AU* auroral electrojet indices, the solar wind number density, the dynamic or ram pressure, the solar wind speed Vsw, and the Bx, By and Bz components of the IMF are shown respectively as panels 1 to 8 in Figures 2 and 3. Figures 4 and 5 are the statistical analysis of the parameters mentioned above. The black dashed lines in the figures indicate the FAST-ESR conjunction time.

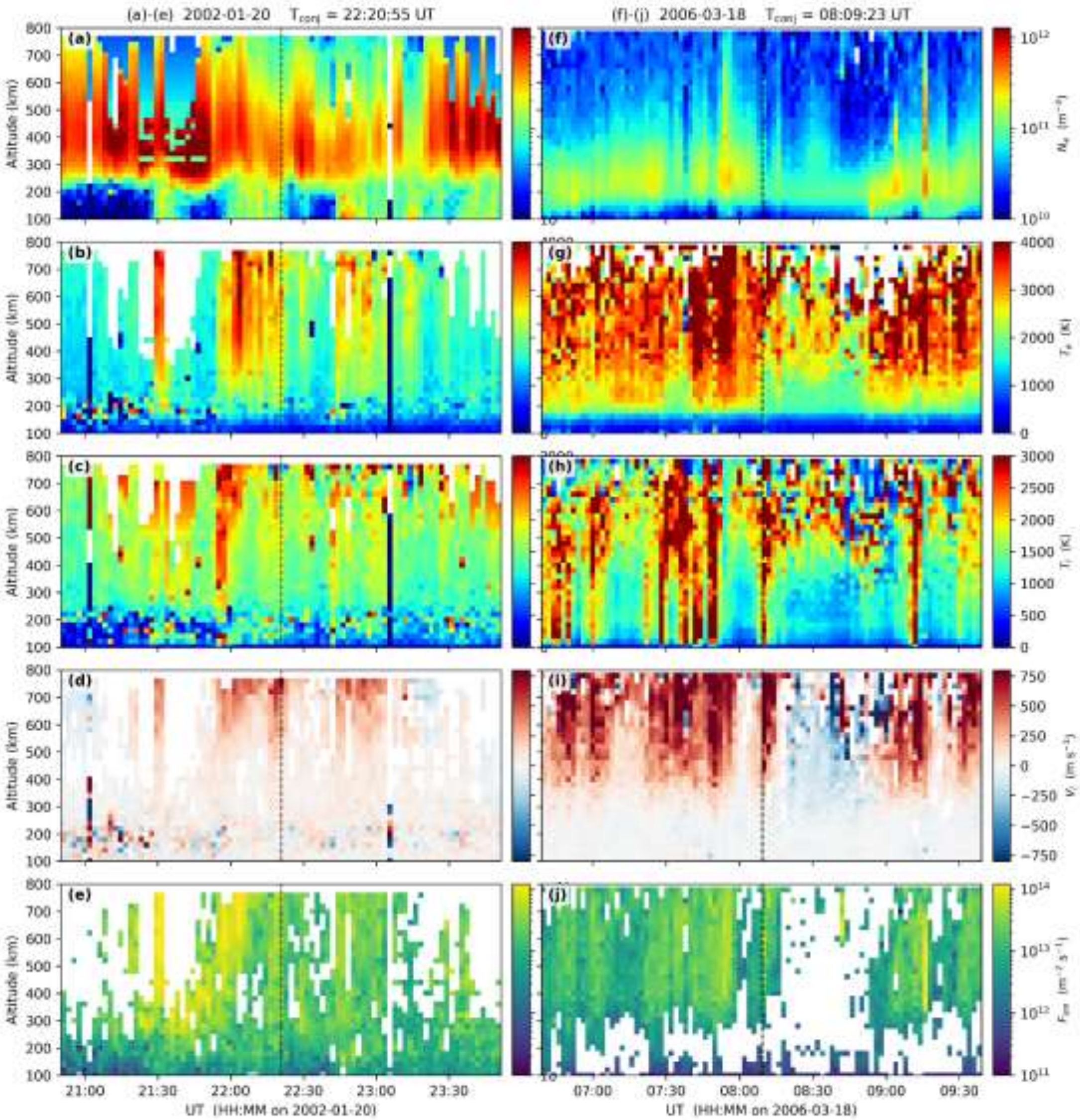

Figure 1: Representative ESR ion-upflow signatures for the two case-study FAST-ESR conjunction events used in this work. (a) 2002-01-20 ($T_{conj} = 22{:}20{:}55\ UT$) and (b) 2006-03-18 ($T_{conj} = 08{:}09{:}23\ UT$). Each panel shows ESR electron density (N_e), electron temperature (T_e), ion temperature (T_i), field-aligned ion drift velocity (V_i) and ion flux (F_{ion}) as a function of altitude and UT, with the dashed line marking the conjunction time. Plotted from ESR data accessed via the EISCAT Madrigal database; the same events are also presented in David et al. [31].

3.1. OMNI Plot

Each of the plots in this section comprises eight panels, namely, the SYM-H ring current index, the AL and AU auroral electrojet indices, the solar wind number density, the dynamic pressure, the solar wind speed

V_sw,and the B_x,B_y and B_z components of the IMF respectively. The plots span six hours including the conjunction time in each of the events.

3.1.1. 2002-01-20 EVENT: Figure 2 presents the OMNI record for the 2002-01-20 nightside conjunction (T_conj=22:20:55 UT). Throughout the displayed window the SYM-H ring-current index remains weakly negative (typically > -30 nT), indicating that no significant magnetic storm developed during the conjunction interval. The auroral electrojet panel shows fluctuations of AL in the -90 to -150 nT range until ~20:50 UT, after which a sharp negative excursion to magnitudes greater than -350 nT occurs. This rapid intensification of the westward auroral electrojet is the standard signature of substorm expansion-phase onset [27, 28]. Inspection of the IMF B_z panel shows that the field had been continuously southward for ~1 h prior to onset, reaching a minimum near 19:50 UT before recovering toward weakly negative values. This sustained southward orientation provides the > 30 min loading of open flux into the magnetotail required to support a subsequent expansion phase under the Cowley-Lockwood paradigm [27]. We note that, contrary to a common misreading, the negative AL excursion accompanying expansion onset reflects the closure (not the destruction) of previously opened flux as nightside reconnection proceeds, with the energy stored during the growth phase being released into the auroral ionosphere [27]. The conjunction therefore captured ion upwelling above the ESR during a substorm expansion phase under quiet ring-current conditions, in line with the substorm-driven ion energisation pathway described by Strangeway et al. [15] and Wright et al. [14].

3.1.2. 2006-03-18 EVENT: Figure 3 presents the OMNI record for the 2006-03-18 dayside conjunction (T_conj=08:09:23 UT). The IMF B_z panel shows two southward turnings of comparable amplitude separated by a brief recovery, a structure consistent with a stream-interaction event rather than a fully developed two-step magnetic storm in the sense of Kamide et al. [29]. The SYM-H response is correspondingly modest, transitioning from quiet conditions to a weak depression and indicating that the magnetosphere did not enter the main phase of a major storm during the conjunction window. Coincident with the southward B_z intervals, the auroral electrojet panel shows enhanced magnitudes of both AL and AU, indicating active convection driven by enhanced dayside reconnection.

A corotating interaction region (CIR) is identifiable in the solar wind density and dynamic pressure panels between approximately 07:30 and 08:00 UT, where the interface between slow and fast streams produces a sharp pressure pulse and density compression. CIRs are an established class of upstream driver capable of producing extended high-latitude convection enhancements and ion outflow [3]. The combination of CIR-driven solar wind compression and southward IMF therefore provided the conditions for enhanced dayside reconnection and Joule heating during the 2006-03-18 conjunction; this is consistent with the cusp-displacement signature reported for the same event by David et al. [31] and with the upflow flux response described by Strangeway et al. [15] and Ogawa et al. [16]. The geomagnetic disturbance further drives modifications of the thermospheric composition that alter F-region electron concentration on longer timescales [28, 29], although those effects extend beyond the conjunction window analysed here.

3.2. Statistical Analysis

3.2.1. Coupling Function: Figure 4 presents the measure of the energy fraction extracted from the solar wind into the magnetosphere, usually called coupling function, for each of the events. There have been many coupling function formulas relating the quantity of energy extracted, but in this work, Milan et al. [30] approach was employed due to its high Pearson correlation coefficient, ρ, which is a measure of linear correlation between variables.

$$\Phi_D = \Lambda V_x^{\frac{4}{3}} \; B_{YZ} \, sin^{\frac{9}{2}}\left(\frac{\theta}{2}\right) \tag{3.1}$$

where,

V_x is the speed of the solar wind,

$B_{YZ}^2 = B_Y^2 + B_Z^2$ is the transverse GSM components of the IMF

θ is the clock-angle, the angle between the IMF vector projected into the

GSM Y-Z plane and the Z-axis, i.e., $\theta = \tan^{-1}(\frac{B_Y}{B_Z})$

and Λ is the coefficient of proportionality given by $3.3 \times 10^5\ m^{2/3}\ s^{1/3}$

Bearing in mind that viscous interaction excite convection without the occurrence of dayside reconnection, which gives an offset of order 25 kV in coupling function [30], it could be seen from the plots that some events show weak activity, some moderate while the strongest activities occurred in the 3rd and 6th events, with observed peaks, greater than 200 and 100 kV respectively.

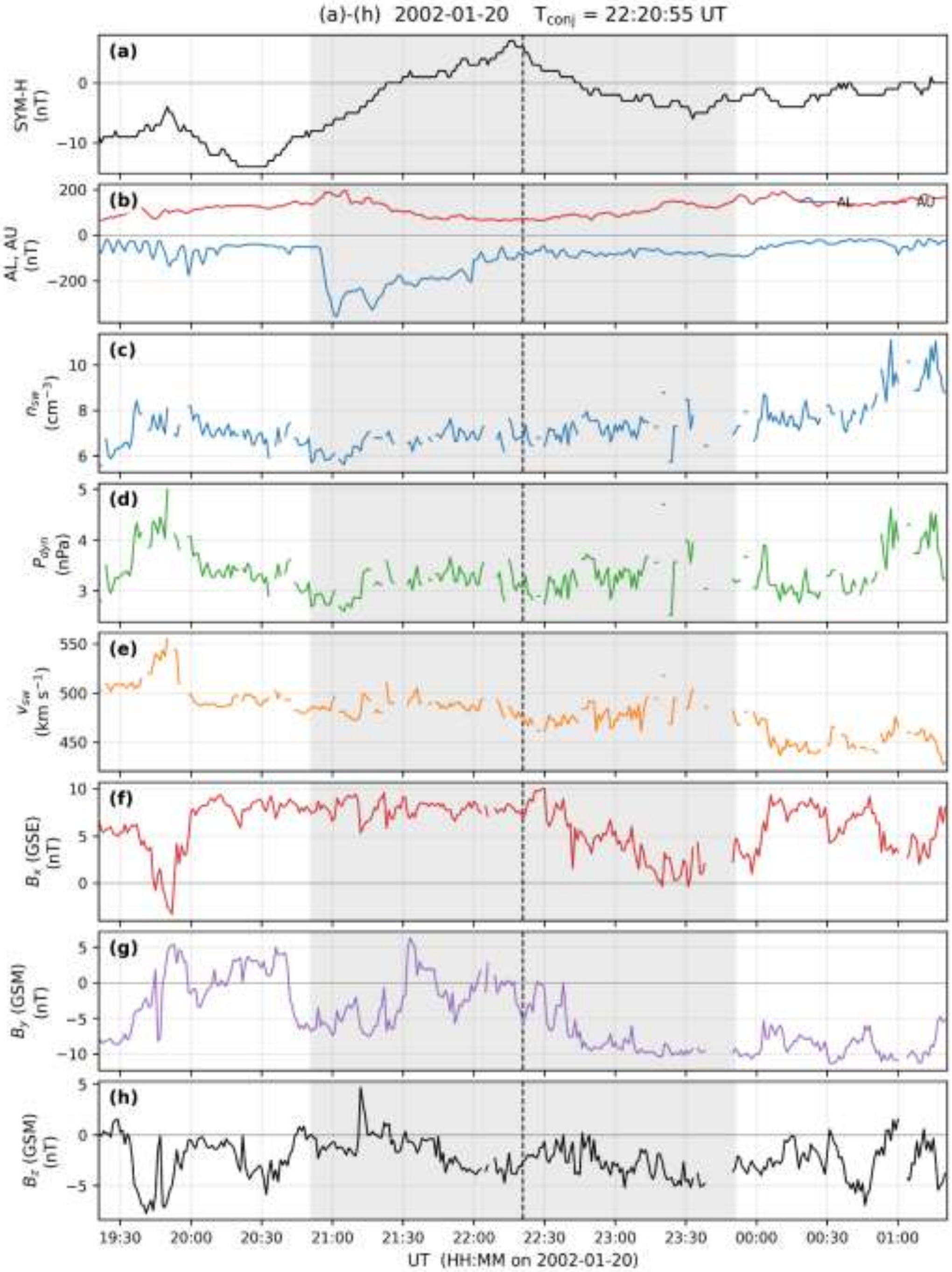

Figure 2: Plot showing the OMNI measurements for the 2002-01-20 conjunction event. The panels from top to bottom are the Sym-H, upper and lower auroral electrojet indices (AU and AL, above and below zero respectively), solar wind density, dynamic pressure, solar wind speed in the GSE

coordinate, $IMF\ B_x, IMF\ B_y, and\ IMF\ B_z$ respectively. The black dashed line indicates the FAST-ESR conjunction.

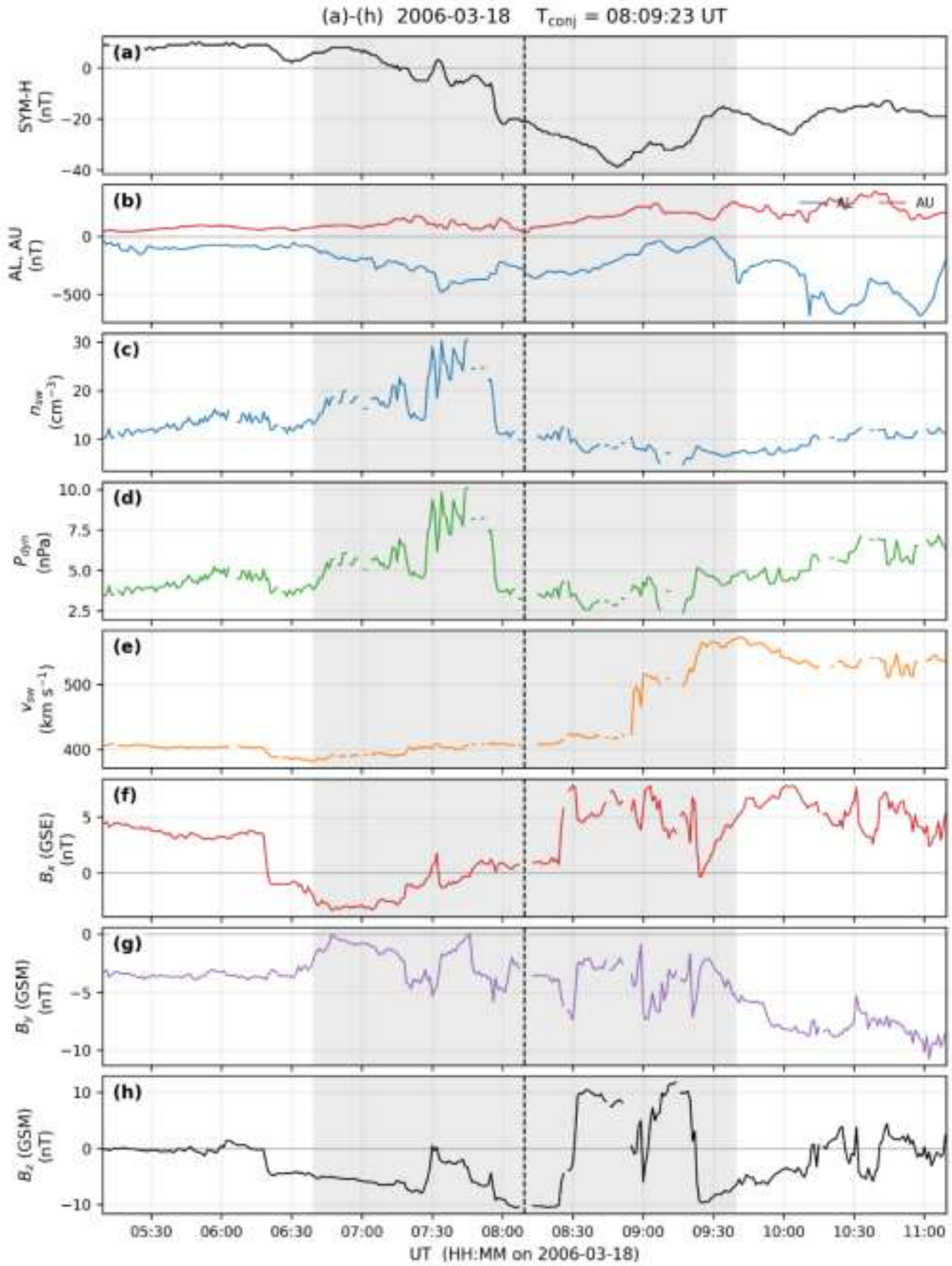

Figure 3: Plot showing the OMNI measurements for the 2006-03-18 conjunction event. The panels from top to bottom are the Sym-H, upper and lower auroral electrojet indices (AU and AL, above and below zero respectively), solar wind density, dynamic pressure, solar wind speed in the GSE coordinate, $IMF\ B_x, IMF\ B_y, and\ IMF\ B_z$ respectively. The black dashed line indicates the FAST-ESR conjunction.

3.2.2. Measures of Central Tendency and Dispersion: Figure 5 summarises the central tendency and dispersion of each parameter across the seven conjunctions. The SYM-H panel is predominantly negative, indicating depressed ring-current conditions during all seven events, with the 2005-09-12 conjunction showing the most negative median and the largest interquartile range. This is the strongest magnetospheric response in the sample and is consistent with this event also showing the largest AL excursion (~ −600 nT) and the largest standard deviation (~ 300 nT) in the auroral electrojet panel, signalling pronounced substorm activity. Conversely, the 2008-02-14 event has the weakest geomagnetic response, which we attribute to its occurrence near the solar minimum of cycle 23/24 when the average solar-wind driver is reduced. Because Q1 and Q3 partition the symmetric ±3 h window about T_conj, they additionally indicate temporal asymmetry: for the 2005-09-12 event the most negative AL values are concentrated before T_conj, whereas for 2005-09-18 and 2008-02-14 the activity is concentrated after, indicating that ion upwelling at these conjunctions was sampled during the recovery and growth phases respectively.

The lower six panels of Figure 5 describe the upstream solar wind conditions. The number density and dynamic pressure panels are nearly stationary at most events, with the conspicuous exception of the 2006-03-18 conjunction, which shows the largest dispersion and the most elevated lower quartile. This is the signature of the corotating interaction region identified in Section 3.1 and visible in Figure 3, in which compression at the slow/fast stream interface drives transient pressure pulses that impinge on the magnetopause. The same event also shows the largest standard deviation in solar wind speed (close to 80 km s^{-1} from the mean), confirming that 2006-03-18 was the most variable upstream event in the sample. The IMF By panel shows that the 2005-09-18, 2006-03-11 and 2008-02-14 conjunctions occurred under duskward IMF, while the remaining four events occurred under dawnward conditions; this asymmetry has implications for the cusp displacement and therefore for the magnetic local time at which dayside upwelling is most efficient [20, 26]. Reconnection driving, as inferred from the IMF Bz panel, is most negative on average for the 2006-03-18 event, in agreement with the coupling-function ranking shown in Figure 4. Taken together, the statistical comparison suggests two distinct upwelling regimes within the sample: a dayside regime that includes both the CIR-driven 2006 03 18 event (elevated dynamic pressure and strong dayside reconnection) and the strong-coupling 2005 09 12 event (highest coupling function, deepest SYM H, largest AL excursion); and a nightside substorm-driven regime, represented in the sample by the 2002 01 20 conjunction, characterised by sustained southward IMF followed by a sharp AL excursion at expansion onset. The remaining four events exhibit weaker driving, in line with the lower coupling function values shown in Figure 4. This statistical picture is consistent with the established physical picture in which Joule heating, soft electron precipitation and ambipolar electric fields driven by reconnection or substorm dynamics elevate ion temperatures and lift the topside ionosphere [14, 15, 17].

4. Conclusions

We have characterised the interplanetary and geomagnetic conditions during seven FAST-ESR magnetic conjunctions for which ion upwelling above the EISCAT Svalbard Radar was previously identified by David et al. [31]. Using one-minute OMNI data we examined the 2002-01-20 nightside conjunction and the 2006-03-18 dayside conjunction in detail, and computed event-by-event central tendency, dispersion and the Milan et al. [30] dayside reconnection coupling function across all seven events.

The 2002-01-20 conjunction sampled ion upwelling during a substorm expansion phase: ~1 h of sustained southward IMF was followed by a sharp negative excursion of AL exceeding -350 nT under weakly negative SYM-H. The 2006-03-18 conjunction sampled ion upwelling during a corotating interaction region with two close southward turnings of B_z, elevated solar-wind density and dynamic pressure, and active dayside auroral convection. The statistical comparison identifies the 2006-03-18 event as the most variable upstream driver in the sample, the 2005-09-12 event as the strongest magnetospheric response, and ranks the seven events into a dayside-driven group (most strongly represented by 2005 09 12 and 2006 03 18) and a nightside substorm-driven event (2002 01 20), with the remaining four conjunctions showing weaker driving consistent with their lower coupling function values.

These results provide a baseline upstream characterisation that complements the ESR-based upflow identifications of David et al. [31]. As a descriptive study, the findings are consistent with the established physical picture in which southward IMF, elevated dynamic pressure and substorm activity favour ion energisation through Joule heating, soft electron precipitation and ambipolar electric fields [14, 15]. The small sample (N = 7) prevents inferential testing, and a future study extending the conjunction set beyond the FAST mission lifetime, for instance using the Cluster or Swarm satellites in conjunction with EISCAT, would enable a quantitative regression between coupling-function strength and ESR-measured upflow flux, refining magnetospheric outflow models and improving space-weather predictive capability.

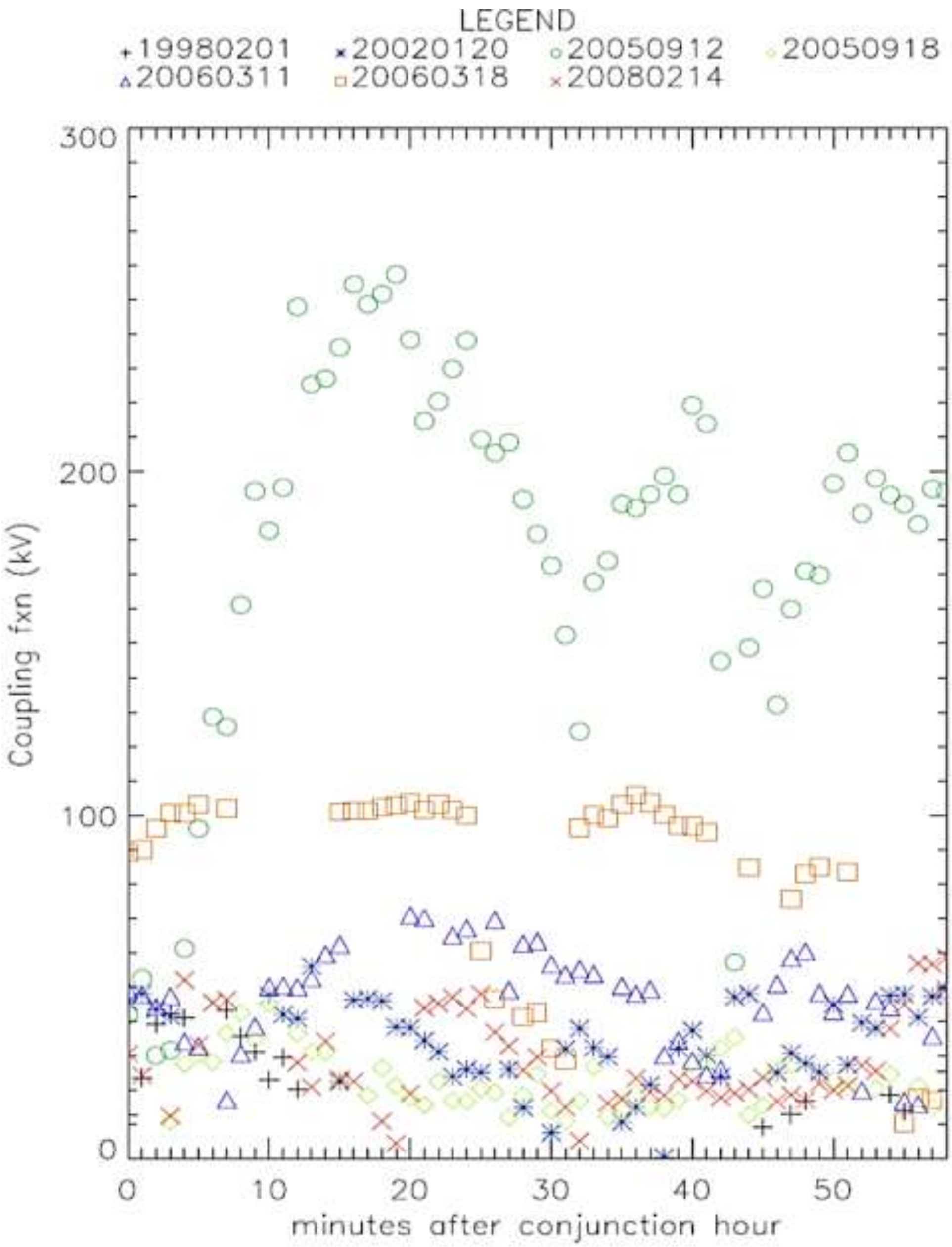

Figure 4: Plot showing the Milan et al. [30] dayside reconnection coupling function for all seven conjunction events listed in Table 1. The colour coded shapes indicate the dates of events as described in the legend of the figure.

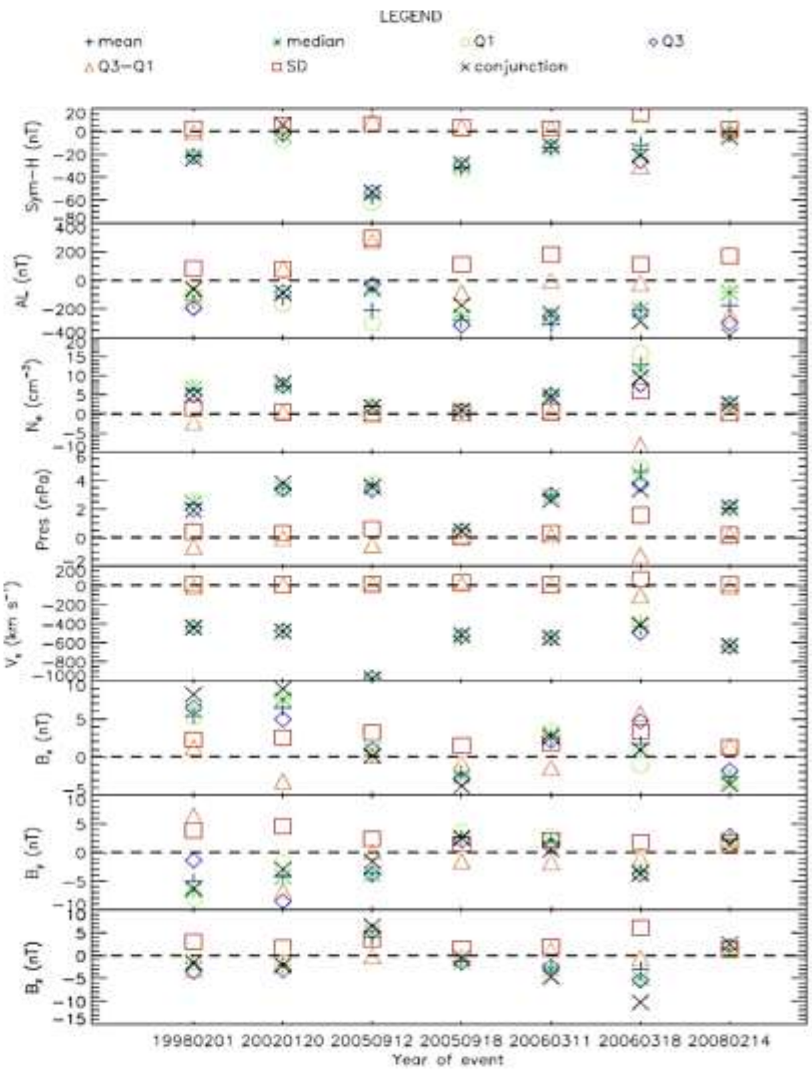

Figure 5: Plot showing the measures of central tendency (mean, median) and dispersion (Q1, Q3, standard deviation) for the seven conjunction events listed in Table 1. The panels from top to bottom are the Sym-H, lower auroral electrojet index (AL), solar wind density, dynamic pressure, solar wind speed in the GSE coordinate, $IMF\ B_x, IMF\ B_y, and\ \ IMF\ B_z$ respectively. The black horizontal dashed lines indicate the horizontal axis at the origin.

Funding: This research did not receive any specific grant from funding agencies in the public, commercial or not-for-profit sectors.

Acknowledgements: OMNI 1-min solar-wind and geomagnetic data were obtained from the NASA Goddard Space Flight Center OMNIWeb service (https://omniweb.gsfc.nasa.gov). EISCAT Svalbard Radar data were obtained from the EISCAT Madrigal database (https://madrigal.eiscat.se). EISCAT is an international association supported by research organisations in China, Finland, Japan, Norway, Sweden and the United Kingdom.

Data availability: All datasets used in this study are publicly available from the OMNIWeb (NASA) and Madrigal (EISCAT) databases as cited above.

Competing interests: The authors declare no competing interests.

REFERENCES

1 Falthammar, C. (1986). Magnetosphere Ionosphere Interactions - Near-Earth Manifestations of the Plasma Universe. *IEEE Transactions on Plasma Science,* **14** 616. https://doi.org/10.1109/tps.1986.4316613

2 Lakhina, G. S., Alex, S. and Rawat, R. (2009). *An Overview of the Magnetosphere, Substorms and Geomagnetic Storms. Turbulence, Dynamos, Accretion Disks, Pulsars and Collective Plasma Processes*, Astrophysics and Space Science Proceedings, Springer, Netherland 293.

3 Kivelson, M. G. and Russell, C. T. (1995). *Introduction to Space Physics (First edition)*. United Kingdom, University of Cambridge: Cambridge University Press.

4 Gonzalez, W. D. and Tsurutani, B. T. (1987). Criteria of interplanetary parameters causing intense magnetic storms ($D_{st} < -100$ nT). *Planetary and Space Science* **35** 1101.

5 David, T. W., Adekoya, B. J., Michael, C. M., Adekoya, S. A., Adenuga, O. A., Kareem,S. O., Oladunjoye, H. T., Ajetunmobi, A. E., Williams, O.T. and Ogundele, D. T. (2022). A Study of the Relationship Between Southward *Bz* > -10 nT and Storm Time Disturbance Index During Solar Cycle 23. *Journal of the Nigerian Society of Physical Sciences* **4(4)** 620-627. https://doi.org/10.46481/jnsps.2022.620

6 Axford, W. I. and Hines, C. O. (1961). A unifying theory of high-latitude geophysical phenomena and geomagnetic storms. *Canadian Journal of Physics* **39** 1433. https://doi.org/10.1139/p61-172

7 Yau, A.W., Shelley, E.G., Peterson, W.K. and Lenchyshyn, L. (1985). Energetic auroral and polar ion outflow at DE-1 altitudes - Magnitude, composition, magnetic activity dependence, and long-term variations. *Journal of Geophysical Research* **90** 8417. https://doi.org/10.1029/ja090ia09p08417

8 Chappell, C.R., Giles, B.L., Moore, T.E., Delcourt, D.C., Craven, P.D. and Chandler, M.O. (2000). The adequacy of the ionospheric source in supplying magnetospheric plasma. *Journal of Atmospheric and Solar-Terrestrial Physics* **62** 421. https://doi.org/10.1016/s1364-6826(00)00021-3

9 Hultqvist, B., Øieroset, M., Paschmann, G., and Treumann, R. A. (1999). Source processes in the high-latitude ionosphere. *In Space sciences series of ISSI* 7–84. https://doi.org/10.1007/978-94-011-4477-3_2

10 André, M. and Yau, A. (1997). Theories and observations of ion energization and outflow in the high latitude magnetosphere. *Space Science Reviews **80**(1-2) 27-48.* https://doi.org/10.1007/978-94-009-0045-5_2

11 Shelley, E.G., Peterson, W.K., Ghielmetti, A.G. and Geiss, J. (1982). The polar ionosphere as a source of energetic magnetospheric plasma. *Geophysical Research Letters* **9**(9) 941-944. https://doi.org/10.1029/gl009i009p00941

12 Dandouras, I. (2013). Detection of a plasmaspheric wind in the Earth's magnetosphere by the Cluster spacecraft. *Annales Geophysicae* **31**(7) 1143-1153. https://doi.org/10.5194/angeo-31-1143-2013

13 Toledo-Redondo, S., André, M., Aunai, N., Chappell, C. R., Dargent, J., Fuselier, S. A., Glocer, A., Graham, D. B., Haaland, S., Hesse, M., Kistler, L. M., Lavraud, B., Li, W., Moore, T. E., Tenfjord, P. and Vines, S. K. (2021). Impacts of ionospheric ions on magnetic reconnection and Earth's magnetosphere dynamics. *Reviews of Geophysics* **59** e2020RG000707 https://doi.org/10.1029/2020RG000707

14 Wright, D. M., Davies, J. A. and Strangeway, R. J. (2012). Observations of ion outflows at high-latitudes derived from ground-based radar and spacecraft measurements. *EGU General Assembly Conference Abstracts, Vienna, Austria*, 6568. http://ui.adsabs.harvard.edu/abs/2012EGUGA..14.6568W/abstract

15 Strangeway, R.J., Ergun, R.E., Su, Y.J., Carlson, C.W. and Elphic, R.C. (2005). Factors controlling ionospheric outflows as observed at intermediate altitudes. *Journal of Geophysical Research* **110** A03221.

16 Ogawa, Y., Buchert, S.C., Fujii, R., Nozawa, S. and van Eyken, A.P. (2009). Characteristics of ion upflow and downflow observed with the European Incoherent Scatter Svalbard radar *Journal of Geophysical Research* **114** A05305. *https://doi.org/10.1029/2008ja013817*

17 David, T.W., Wright, D.M., Milan, S.E., Cowley, S.W.H., Davies, J.A. and McCrea, I. (2018). A study of observations of ionospheric upwelling made by the EISCAT Svalbard Radar during the International Polar

Year campaign of 2007. *Journal of Geophysical Research: Space Physics* **123** 2192-2203. https://doi.org/10.1002/2017JA024802
18 Glocer, A., Toth, G., and Fok, M.-C. (2018). Including kinetic ion effects in the coupled global ionospheric outflow solution. *Journal of Geophysical Research: Space Physics* **123** 2851-2871. https://doi.org/10.1002/2018JA025241
19 Glocer, A., Collinson, G., Garcia-Sage, K., Welling, D., Chappell, C., Rowland, D., Varney, R., Ilie, R. and Kistler, L. (2023). The Outflow and Recirculation of Ionospheric Plasma. *Bulletin of the American Astronomical Society* **55** 130. https://doi.org/10.3847/25c2cfeb.a1163052
20 Howarth, A. and Yau, A. W. (2008). The effects of IMF and convection on thermal ion outflow in magnetosphere-ionosphere coupling *Journal of Atmospheric and Solar-Terrestrial Physics* **70** 2132. https://doi.org/10.1016/j.jastp.2008.08.008
21 Wahlund, J. E. and Opgenoorth, H. J. (1989). EISCAT Observations of Strong Ion Outflows from the F-region ionosphere during auroral activity – Preliminary results. *Geophysical Research Letters*, **16**(7) 727-730 https://doi.org/10.1029/GL016i007p00727
22 David, T. W., Michael, C. M., Awoyinka, T. D., Ajetunmobi, A. E. and Talabi, A. T. (2024). Energetic Ionospheric upwelling: A Case Study of Velocity Distribution and Ion Flux Observed by the EISCAT Svalbard Radar. *International Journal of Energetica* **9**, 48-53 http://dx.doi.org/10.47238/ijeca.v9i2.252
23 David, T. W. (2013). Investigation into Quiet and Magnetic Storms Periods Above Magadan During October - December, 2003. *Indian Journal of Radio & Space Physics* **42** 89-96 https://nopr.niscpr.res.in/handle/123456789/17094
24 David, T. W., Akintola, A. N. and Adekoya, B. J. (2011). Time/Level of Ionospheric Response to Geomagnetic Storm of 25-26 July 1981 at Different Latitudes. *Indian Journal of Radio & Space Physics* **40** 311-319 https://nopr.niscpr.res.in/handle/123456789/13318
25 David, T. W. and Chukwuma, V. U. (2012). Response of Ionospheric foF2 over South East Asian Sector to Geomagnetic Storm of 29 October 1973 *Indian Journal of Radio & Space Physics* **41** 332-338 https://nopr.niscpr.res.in/handle/123456789/14371
26 Foster, C., Lester, M. and Davies, J.A. (1998). A statistical study of diurnal, seasonal and solar cycle variations of F-region and topside auroral upflows observed by EISCAT between 1984 and 1996. *Annales Geophysicae* **16** 1144-1158 https://doi.org/10.1007/s00585-998-1144-0
27 Lockwood, M. and Cowley, S. W. H. (1992). Ionospheric convection and the substorm cycle, *SUBSTORMS 1: Proceedings of the International Conference on Substorms*, 23-27 March, 1992 https://centaur.reading.ac.uk/38835/

28 Danilov, A. (2001). F2-region response to geomagnetic disturbances. *Journal of Atmospheric and Solar-Terrestrial Physics* **63** 441-449 https://doi.org/10.1016/s1364-6826(00)00175-9
29 Liu, J., Zhao, B. and Liu, L. (2010). Time delay and duration of ionospheric total electron content responses to geomagnetic disturbances. *Annales Geophysicae* **28** 795-805 (2010). https://doi.org/10.5194/angeo-28-795-2010
30 Milan, S. E., Gosling, J. S. and Hubert, B. (2012). Relationship between interplanetary parameters and the magnetopause reconnection rate quantified from observations of the expanding polar cap. *Journal of Geophysical Research: Space Physics* **117** A03226 https://doi.org/10.1029/2011ja017082
31 David, T. W., Adetunji, E. O., Michael, C. M., Wright, D. M., Talabi, A. T., & Ajetunmobi, A. E. (2025). Upwelling Ion Observation from the Earth's Upper Atmosphere During EISCAT Svalbard Radar and FAST Satellite Conjunctions. Nigerian Journal of Physics, **34(4)** 1-13. https://doi.org/10.62292/10.62292/njp.v34i4.2025.198